# The synthesis and characterization of novel multiferroic materials

Bachelor thesis

Author: Joshua Levinsky Student number: S2372169

Supervisor: Dr. G.R. Blake

Second assessor: Prof. Dr. T.T.M. Palstra

Date: 7-7-2015

University of Groningen
**Zernike Institute**
**for Advanced Materials**

# Summary

In this bachelor research project an attempt was made at synthesizing cobalt jarosite and mixed-valent iron jarosite crystals by hydrothermal methods, as previously reported by Rao et al. and Powell et al.
[14,13]. The target compounds were not obtained but three new crystals (two cobalt compounds and one iron compound) were synthesized that are not found in the literature or crystallographic databases. The crystal structure of the two cobalt compounds has been fully solved using single crystal x-ray diffraction. Magnetic susceptibility measurements showed that the obtained pink crystal showed ferromagnetic ordering below 11 K and the obtained orange crystal showed paramagnetic behavior. This behavior was expected based on the crystal structures of the compounds. The magnetic effective moment of the pink crystal was 2.3 $\mu_B$ per Co atom, which was pretty consistent with the theoretical value expected for a low spin $Co^{2+}$ complex. The magnetic effective moment of the orange crystal was 4.7 $\mu_B$ per Co atom which was consistent with the theoretical value expected for a high spin $Co^{3+}$ complex. The magnetization versus applied magnetic field measurement of the pink crystal showed no signs of hysteresis which is consistent with behavior shown by a similar 2D ferromagnetic material. The capacitance measurement of the pink crystal showed a possible structural phase transition at 90 K. A small peak at 90 K in the plotted loss versus temperature indicates that is a genuine anomaly. The crystal structure of the iron compound has not been fully solved and a tentative solution of the crystal structure was made. Magnetic susceptibility measurements showed that this crystal showed paramagnetic behavior.

# 1. Introduction

The term multiferroic was first used in 1994 by H. Schmid to describe materials which possess two or more ferroic orders at the same time.[15] The four types of ferroic order are ferroelectricity, ferromagnetism, ferroelasticity and ferrotorroidicity.[15] Of special interest are multiferroic materials which are ferromagnetic and ferroelectric, although in this case the definition is often extended to include any type of magnetic order. So called magnetoelectric multiferroic materials possess these two ferroic orders and show a net electrical polarization when a magnetic field is applied and vice versa.[15,16] This relationship between magnetic moment and electric polarization was first conjectured by P. Curie in 1894.[3] Research on magnetoelectric multiferroic materials has been ongoing since the 1960s.[7] There are a number of envisaged applications for these kinds of materials including in spintronics and as high sensitivity magnetic field sensors.[11] Spintronics is short for spin transport electronics and this could be used for future data storage technology.[10] The amount of research on magnetoelectric materials, after an initial burst of interest, slowed down until the early 2000s. Interest in magnetoelectric materials was sparked again by research done in 2003 by Kimura et al. who synthesized a magnetically frustrated material, TbMnO3, which showed strong magnetic and electrical coupling.[9]

One big challenge is to find room-temperature multiferroics. The magnetoelectric coupling in most known multiferroics is driven by magnetic frustration, which usually suppresses magnetic transitions down to low temperatures.[2] Furthermore, the magnetoelectric effect in currently known materials is still too weak for it to be used in some applications.[5] In 2009 Mostovoy et al. suggested a way of strengthening the magnetoelectric effect in materials. It was proposed that by combining the breaking of symmetry in magnetic vortices and superexchange mediated spin-lattice coupling, the magnetoelectric effect could be increased.[5] These phenomena can be combined in the smallest magnetic vortex there is, a triangle with antiferromagnetically coupled spins. This structure can be found in nature, for example in a class of compounds called jarosites. Jarosites have a kagome lattice (shown in figure 1) which is made up of corner sharing triangles.[5] This lattice and jarosites in general are renowned for having a geometrically frustrated magnetic system. In iron jarosite ($KFe^{III}_3(OH)_6(SO_4)_2$) where the $Fe^{3+}$ cations form a kagome lattice and in which anionic hydroxy groups form superexchange pathways with the iron cations, no linear magnetoelectric was found.[1] This can be explained in terms of symmetry. In order for a net polarization to exist in a kagome lattice the oxidation states of the cations must be mixed or the symmetry of the system has to be lowered in some other way. The electric dipole moments would otherwise all cancel each other out due to the high symmetry of the system.

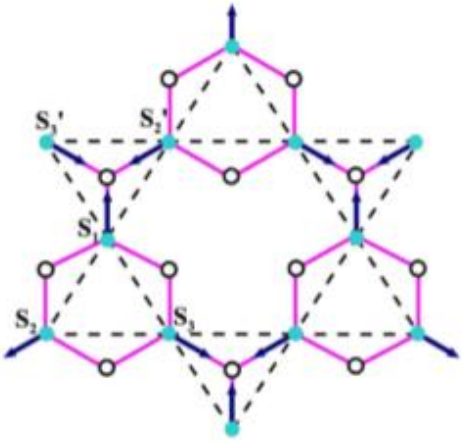


*Figure 1 Sketch of a kagome lattice. The green dots represent magnetic cations and the white dots represent anions.[5]*

This is illustrated in figure 2 where under an externally applied magnetic field the hydroxyl ligands shift in such a way that the electric displacements cancel each other out.[1]

Several people have tried and succeeded in making jarosites via hydrothermal synthesis that show complex magnetic behavior. Several magnetically frustrated jarosites that possess the kagome lattice have been synthesized, for example by Powell et al. and Rao et al.[13,14] Powell synthesized a cobalt jarosite ($Co^{II}_3(SO_4)_3(OH)_2[enH_2]$) which showed some structural differences from the iron jarosite. Despite Co being in a single oxidation state, there are two distinctly different Co-Co linkage distances.[13] This means that the structure has lower symmetry than the iron jarosite and could possibly show magnetoelectric coupling. A mixed-valent iron jarosite ($[HN(CH_2)_6NH][Fe^{III}Fe^{II}_2F_6(SO_4)_2]\cdot[H_3O]$) has been synthesized by Rao et al. which might also meet the requirements for a magnetoelectric multiferroic material. It is also a magnetically frustrated system in which the mixed-valent iron cations lower the symmetry of the system.[14]

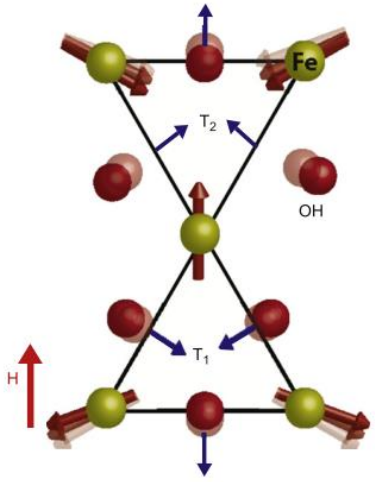


*Figure 2 Sketch of two coupled spin-triangles of iron jarosite in an applied magnetic field. Red arrows denote Fe spins on the triangular apices. Ligand shifts are confined to the plane of the paper. Local dipole moments that cancel out are shown in blue.[1]*

## 1.1 Aim of research

Only the magnetic properties of the cobalt jarosite and mixed-valent iron jarosite have been investigated by Powell and Rao et al. respectively. The possibility of magnetoelectric coupling has not yet been investigated in these materials. The aim of the research that was conducted for my bachelor research project was therefore to synthesize these interesting materials via hydrothermal synthesis and to investigate their magnetic and electric properties as well as investigating if there is any interaction between their magnetic and electrical properties. Another goal was to investigate what impact increasing the pressure of the hydrothermal synthesis had on the formation of the crystals. In the case of the cobalt jarosite synthesis, the effect of varying the molar ratios of the starting materials on the crystals that formed via hydrothermal synthesis was also investigated.

# 2. Theory

It has been proposed by Mostovoy et al. that combining the two phenomena of symmetry breaking in magnetic vortices and superexchange mediated spin-lattice coupling in a material would lead to an increase in the magnitude of the magnetoelectric effect, which is weak in currently known magnetoelectric multiferroic materials.[5] This might be realized in a class of materials known as the jarosites, which possess a geometrically frustrated magnetic kagome lattice.

## 2.1 Geometrically frustrated magnets

Geometric frustration refers to conflicting inter-atomic forces in a crystal which lead to a multitude of ground states for the system.[4] Geometric frustration is found in triangular lattices with magnetic cations where the spins are coupled antiferromagnetically.[4] In figure 3a a triangular lattice is shown where the spins are placed in an antiferromagnetic fashion. The spins labeled 1 and 2 are antiparallel to each other. The orientation of the spin of the third cation cannot satisfy the condition of antiferromagnetism, where the spins are all antiparallel to each other. The energy of the ground state of the system is the same whether the spin is antiparallel to spin 1 or spin 2. Because of this frustration, the magnetic ground state of such a system is a 120˚ spin-star arrangement[1] shown in figure 3b.

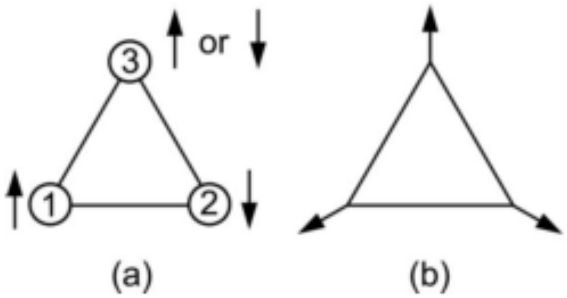


*Figure 3a & 3b (a) The condition of antiferromagnetism cannot be satisfied in this frustrated system.[4] (b) The 120˚ spin-star arrangement is the magnetic ground state for such a frustrated system.[4]*

This spin-star arrangement can also be seen as a magnetic vortex. It has been known for quite some time that spiral magnetic order can lead to an electric polarization when a magnetic field is applied.[5,9,2] The situation is similar for a magnetic vortex, which is illustrated in figure 4a for a perfectly symmetric magnetic vortex. When an external magnetic field is applied (figure 4b), the symmetry of the vortex is broken and a net electric polarization is created. The magnetoelectric repsonse is proportional to the vortex density and that is why the largest magnetoelectric effect is expected from a lattice made up of triangles with antiferromagnetically coupled spins, which are the smallest possible magnetic vortices.[5]

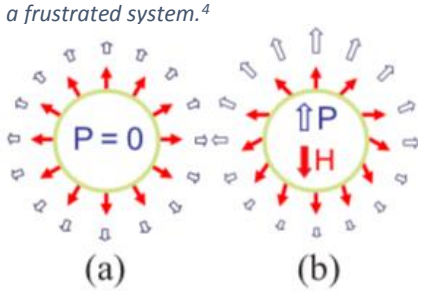


*Figure 4a & 4b Red arrows indicate orientation of spins and blue arrows indicate direction and magnitude of dipole moments. (a) Perfectly symmetric magnetic vortex. (b) When a magnetic field is applied, a net electric polarization is acquired. [5]*

These frustrated triangular systems are very susceptible to small perturbations such as externally applied magnetic fields, which can lead to drastic changes in the ground state of the system.[1] This has certain implications for superexchange pathways and magnetoelectric coupling which will be explained below.

## 2.2 Superexchange mediated spin-lattice coupling

The term superexchange denotes the coupling between two magnetic cations through a non-magnetic anion (often $O^{2-}$). A schematic view of a typical superexchange situation is shown in figure 5a.

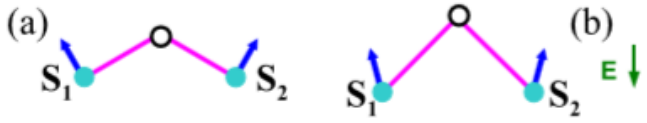


*Figure 5a & 5b (a) Typical superexchange situation where two magnetic cations (green dots) are coupled through a non-magnetic anion (white dot).[5] (b) When an external electric field is applied, the ions with opposing charges shift away from each other.[5]*

Because of the opposing charges of the cations and ligand, they shift away from each other when an external electric field is applied (seen in figure 5b). The metal-oxygen-metal angle (θ), is hence changed by this electric field. This means that the interaction between the spins is also altered. According to the Goodenough - Kanamori rules, when θ=90˚ the magnetic exchange is ferromagnetic and when θ=180˚ the exchange is antiferromagnetic. So by applying an external electric field, the magnetic exchange between the cations is changed.[5] Conversely, changing the spin orientation by an applied magnetic field will alter the electric dipole moment associated with the cation-ligand-cation linkage.

The frustrated nature of the triangular lattice of jarosites has an effect on these superexchange pathways. When an external magnetic field is applied to a frustrated triangular system, the spins will adjust to the magnetic field by small rotations. In the case of an isolated triangle of spins, this removes the local three-fold rotation axis.[1] The lattice then relaxes in response to the spin rotations and the metal-oxygen-metal angles are changed. The oxygen anions move away from or towards the metal–metal axes, creating a net electric dipole moment.[1] Whether or not the dipole moments associated with individual triangles cancel depends on the overall symmetry of the structure – in a kagome lattice there will be no net polarization if the triangles are equilateral.

# 3. Materials and methods

Experimental procedure synthesis jarosites

Hydrothermal synthesis is a crystal growth method where crystals are grown from solution under high pressures and temperatures. This method has the advantage of producing a variety of crystals, often phases that would be difficult to synthesize under ambient conditions. Here two different syntheses were performed. The syntheses were carried by following previous reports.[13,14]

## 3.1 Cobalt jarosite

The attempted synthesis of the cobalt jarosite was carried under hydrothermal conditions under elevated temperature and autogenous pressure in a Parr 4745 acid digestion bomb autoclave with a 23 mL Teflon beaker insert. The starting materials $CoSO_4 \cdot 7H_2O$, $H_2SO_4$, $H_2O$ and ethylenediamine were added to the insert. Eight batches were made, all with different reaction conditions. Four batches contained different quantities of starting materials and four batches had varying molar ratios of the starting materials. In table 1 the contents of the Teflon insert for every batch are shown.

*Table 1 The amount of starting material per batch, what crystals formed per batch and the molar ratios of the starting materials are shown in this table.*

| *Batch* | *1* | *2* | *3* | *4* | *5* | *6* | *7* | *8* |
|---|---|---|---|---|---|---|---|---|
| *$CoSO_4 \cdot 7H_2O$ (g)* | 1.1265 | 5.6005 | 2.8054 | 4.2024 | 5.6212 | 2.8278 | 5.6248 | 2.1832 |
| *Ethylenediamine(g)* | 0.2904 | 1.2161 | 0.6171 | 0.9075 | 0.6201 | 1.2342 | 0.3086 | 0.3102 |
| *$H_2SO_4$ (g)* | 0.4303 | 2.015 | 1.0757 | 1.6135 | 1.0843 | 2.1514 | 1.0803 | 1.0764 |
| *$H_2O$ (g)* | 0.0775 | 0.3555 | 0.1803 | 0.2751 | 0.3660 | 0.1810 | 0.1803 | 0.3655 |
| *N mmol* | 4 | 20 | 10 | 15 | 10 | 10 | 10 | 10 |
| *Crystals formed (**1**, **2** or **3**)* | **1**, **2**, **3** | **1**, **2**, **3** | **1**, **2**, **3** | **1**, **2**, **3** | **1, 2** | **1, 2** | **1, 2** | **1, 2** |
| *Molar ratios* | 1:1:1:1 | 1:1:1:1 | 1:1:1:1 | 1:1:1:1 | 2:1:1:2 | 1:2:2:1 | 2:0.5:1:1 | 1:0.5:1:2 |

The autoclave containing the Teflon insert was then heated over 3 hours in a furnace to 443 K and held at this temperature for 5 days under autogenous pressure. After 5 days the autoclave was cooled down to room temperature over 3 hours. The obtained crystals were washed with methanol.

## 3.2 Mixed-valent iron jarosite

The attempted synthesis of the mixed-valent iron jarosite was carried out under hydrothermal conditions under elevated temperature and autogenous pressure in a Parr 4745 acid digestion bomb autoclave with a 23 mL Teflon beaker insert. The starting materials ferric citrate, $H_2SO_4$, $H_2O$, DABCO (1,4-diazabicyclo[2.2.2]octane), $NH_4F \cdot HF$ (AF875-125 mixture containing 6 wt.%

HF) and n-butanol were added to the insert. Three batches were made with different quantities of starting material. In table 2, the contents of the Teflon insert for every batch are shown.

*Table 2 The amount of starting material per batch is shown in this table.*

| Batch | 1 | N mmol | 2 | N mmol | 3 | N mmol |
|---|---|---|---|---|---|---|
| Ferric citrate (g) | 0.2505 | 1 | 0.4823 | 2 | 0.3696 | 1.5 |
| $H_2SO_4$ (g) | 0.3920 | 4 | 0.8096 | 8 | 0.6052 | 6 |
| DABCO (g) | 0.6624 | 6 | 1.3513 | 12 | 1.0202 | 9 |
| $H_2O$ (g) | 0.8995 | 50 | 1.8225 | 100 | 1.3646 | 75 |
| $NH_4F{\cdot}HF$ (g) | 1.4154 | 4 | 2.7059 | 8 | 1.9917 | 6 |
| n-butanol (g) | 2.2496 | 30 | 4.4294 | 60 | 3.3995 | 45 |

The autoclave containing the Teflon insert was then heated over 3 hours in a furnace to 453 K and held at this temperature for 2 days under autogenous pressure. After 2 days the autoclave was cooled down to room temperature over 3 hours. The obtained crystals were washed with ethanol.

## 3.3 Characterization

Single crystal x-ray diffraction:

The crystals that were obtained via the hydrothermal synthesis were identified and characterized using single crystal x-ray diffraction. This was performed using a Bruker D8 Venture diffractometer with a Photon100 CMOS detector and operating with Mo Kα radiation. All measurements were carried out at 100 K to minimize the Debye-Waller factors and obtain the best possible diffracted signal.

## 3.4 Magnetic measurements

A Quantum Design MPMS-7 SQUID magnetometer was used for measuring the magnetic properties of the obtained crystals. The SQUID magnetometer (Superconducting Quantum Interference Device) is comprised of two pairs of superconducting coils separated by a thin insulating layer. Cooper pairs of electrons can tunnel from one superconductor to the other via these junctions. A sample moving through the coils will cause a change in magnetic flux. When the current is kept constant in the device, the measured voltage oscillates with the changes in phase at the junctions. By counting the oscillations, one can determine the change in flux. One period of voltage variation corresponds to one flux quantum. In this way a SQUID is used to convert the change in magnetic flux into voltage. From this, one can determine the magnetic moment of a sample. The method that was used in all the magnetic susceptibility measurements shown here is known as the RSO (reciprocating sample oscillation) method.

Here the sample is moved sinusoidally and continuously through the coils during a measurement. This reduces the noise contribution and makes this method very sensitive.

## 3.5 Sample preparation & measurements

The samples were attached to a straw using Mylar tape (shown in figure 6 below) and their zero field cooled and field cooled magnetic susceptibilities were measured over the temperature range from 5 to 300 K with an externally applied magnetic field of 1000 Oe. The magnetization versus applied field was also measured for one crystal at 5 K. The magnetic field was not aligned to a particular crystal direction. The crystals obtained from the attempted iron jarosite synthesis were very small and hence many were put in a gel capsule filled with cotton wool, which was inserted into the straw. No correction for the diamagnetic contributions of the cotton and gel capsule was made to the data.

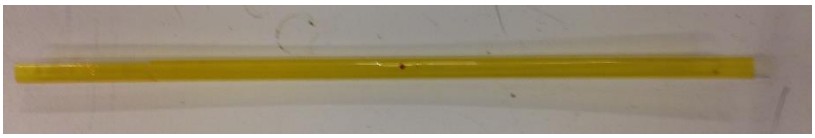

*Figure 6 A crystal attached to a Mylar tape covered straw.*

## 3.6 Data analysis

The magnetic susceptibility of the crystals in the paramagnetic region was fitted using the Curie-Weiss law (equation 1).

*(Equation 1)*

$$\chi = \frac{C}{T-\theta}$$

In this formula:

χ = magnetic susceptibility (dimensionless but often expressed in terms of molar susceptibility with its unit being emu/mol.Oe)
C = Curie constant
T = Temperature (K)
Θ = Weiss constant (K)

A plot of the inverse susceptibility versus temperature is linear in this regime and allows C and θ to be obtained. The value of the Weiss constant is an indicator of what kind of magnetic

interactions are dominant in the material and how strong these interactions are. If the Weiss constant is zero, the magnetic ions do not interact. In such a case, the magnetic susceptibility is proportional to 1/T. When the Weiss constant has a negative value, antiferromagnetic interactions between cations dominate, and when the Weiss constant has a positive value, ferromagnetic interactions dominate.

The effective magnetic moment of a material can be calculated from the Curie constant (the product of the molar susceptibility and the temperature).[8] This is shown below in equation 2. The theoretical value of the effective moment is shown in equation 3.

*(Equation 2)*

$$\mu_{eff} = \sqrt{\frac{3k}{N{\mu^2}_B}}\sqrt{T\chi} \approx \sqrt{8T\chi}$$

*(Equation 3)*

$$\mu_{eff} = 2\sqrt{S(S+1)}$$

## 3.7 Electrical properties measurement

*Figure 7 PPMS equipment.*

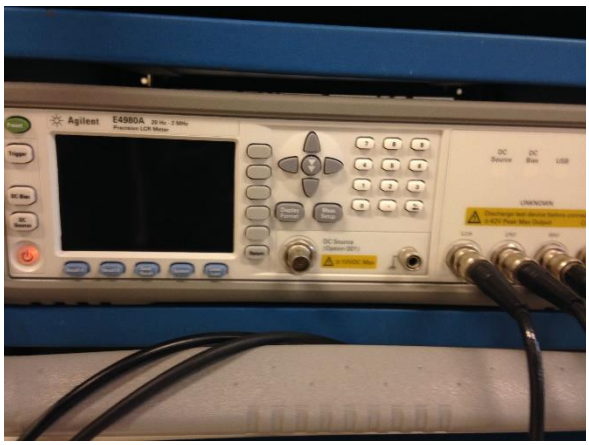


*Figure 8 Agilent E4980A LCR meter.*

The capacitance of one of the crystals obtained from the attempted cobalt jarosite synthesis was determined using an Agilent E4980A LCR meter (shown in figure 8 above) that uses the auto balancing bridge method. The temperature and magnetic field were controlled using a PPMS (Physical Properties Measurement System), shown in figure 7.

## 3.8 Sample preparation & measurement

For the measurement of capacitance, the crystal was fixed vertically on a sample holder (shown in figure 9) and two thin platinum wires were soldered to the sample holder contacts. Contacts were made on opposite sides of the crystal with silver paint and were soldered to the two platinum wires using silver paint.
The capacitance (Cp) and corresponding loss factor (D) were measured for frequencies between 100 Hz and 1 MHz on warming from 5 K to 300 K in 5 K steps, either in zero applied magnetic field or in an applied magnetic field of 5T.

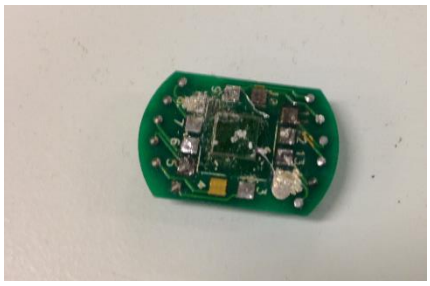

*Figure 9 Sample holder for electrical measurements on which a crystal has been mounted that has been connected to two contacts.*

# 4. Results and discussion

## 4.1 Attempted cobalt jarosite synthesis

*Figure 10 Orange colored crystals of compound **2***

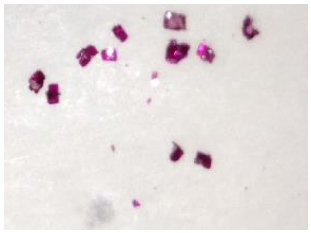

*Figure 11 Pink colored crystals of compound **3***

Three different crystals, transparent, orange and pink in color, were obtained from the attempted synthesis of the cobalt jarosite (see table 2). After determining the unit cells of the crystals using single crystal x-ray diffraction, it was found that only the transparent crystal was already documented in the literature. The lattice parameters of this crystal corresponded to those reported for ethylenediammonium sulphate $(C_2H_4N_2H_6)SO_4$ (compound **1**). The lattice parameters of the orange (compound **2**) and pink (compound **3**) crystals did not match any found in the literature or in crystallographic databases. Figure 10 shows a picture of the obtained orange crystals **2**, the largest of which were about 5mm x 2mm x 2mm in size. Figure 11 shows the obtained pink crystals **3**, the largest of which had dimensions of about 1mm x 1mm x 0.2mm and a plate-like shape.
Batches 1 through 4 all produced these three crystals even though the total quantities of the starting materials were different in every batch. Therefore, increasing the pressure that is present during the hydrothermal synthesis does not seem to have any effect on which crystals are formed. In batches 5 through 8, where the molar ratios of the starting materials was varied, only the orange crystals were produced. The 1:1:1:1 molar ratio that was used in the experimental procedure of Powell et al. seems to be the only way of producing crystals with a similar structure to that of the target cobalt jarosite. The actual temperature of the oven that was used for hydrothermal synthesis is not precisely known since it has not been calibrated. The actual temperature of Powell's oven is also not known and therefore it is not clear if varying the temperature at which the synthesis takes place, could produce the target cobalt jarosite.

## 4.2 Single crystal x-ray diffraction results

Orange crystals **2**:

The crystal structure of a crystal of **2** was determined using single crystal x-ray diffraction. A total of 3082 reflections were collected and the structure was solved and refined in the spacegroup P-1. The chemical composition of **2** was determined to be $Co(SO_4)_2[enH_2]\cdot 4H_2O$. From charge balance considerations the ethylenediamine molecules are likely tobe doubly protonated. $R(F^2)$ was 0.0272 for 2945 reflections with intensities greater than 4 times their standard deviations and 0.0285 for 3082 reflections. This means that the X-ray intensities calculated from the model structure agree extremely well with those measured. The structural information for this crystal is shown below in table 3 and the Co-O bond distances are shown in table 4. The atomic coordinates and temperature factors can be found in Appendix B.

*Table 3 Structural information for compound **2.***

| *Formula* | *$Co(SO_4)_2[enH_2]\cdot 4H_2O$* |
|---|---|
| *Molar mass (g/mol)* | 385.2337 |
| *Crystal system* | Triclinic |
| *Space group* | P-1 |
| *a (Å)* | 6.7957(5) |
| *b (Å)* | 7.0252(5) |
| *c (Å)* | 7.2100(5) |
| *α (°)* | 74.885(3) |
| *β (°)* | 72.117(3) |
| *γ (°)* | 79.329(3) |
| *V ($Å^3$)* | 314.17(4) |
| *Z* | 1 |

*Table 4 Co-O bond distances*

| *Atoms 1,2* | *d 1,2 (Å)* |
|---|---|
| *Co1—O4* | 2.0738(10) |
| *Co1—O1* | 2.0981(9) |
| *Co1—O3* | 2.1122(9) |

The unit cell of this crystal was drawn using the Diamond - Crystal and Molecular Structure Visualization software and can be seen below in figure 12.

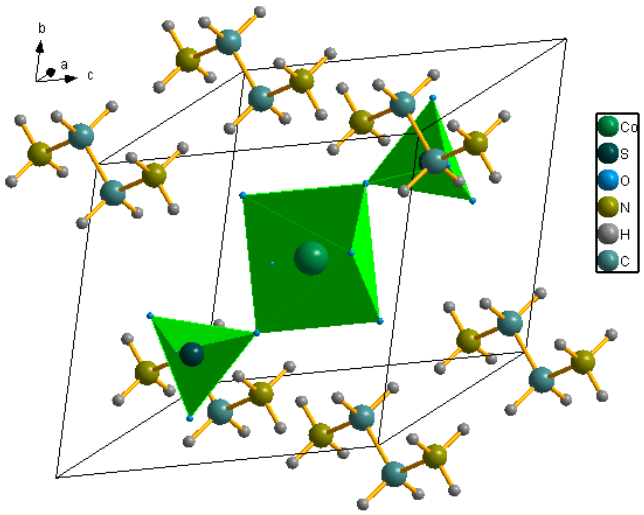


*Figure 12 Representation of the unit cell of compound **2***

The middle of the unit cell contains an isolated $CoO_6$ octahedron where Co is surrounded by four $H_2O$ equatorial ligands (positions of hydrogen atoms not determined) and two sulphate axial ligands. The Co-O distances range from 2.07 to 2.11 Å which is a little higher with $Co^{3+}$ distances found in for example $LaCoO_3$ (1.87-1.99Å)[6] The isolated cobalt octahedron suggests that this crystal will show paramagnetic behavior due to the large distances between cobalt

cations (6.80-7.03Å). These distances are too great for significant magnetic interactions to be present.

Pink crystals **3**:

The crystal structure of a pink crystal **3** was also determined using single crystal x-ray diffraction. The chemical composition of **3** was determined to be $Co_4(OH)_6(SO_4)_2[enH_2]$. From charge balance considerations the ethylenediamine molecules are likely tobe doubly protonated. A total of 5843 reflections were collected and the structure was refined in the spacegroup P-1. R(F) was 0.0721 for 3254 reflections with intensities greater than 4 times their standard deviations and 0.1215 for all 5843 reflections. The structural information for this crystal is shown in table 6 and the Co-O bond distances are shown in table 5. The atomic coordinates and temperature factors can be found in Appendix A.

*Table 5 Co-O bond distances*

| *Atom 1,2* | *d 1,2 [Å]* | *Atom 1,2* | *d 1,2 [Å]* | *Atom 1,2* | *d 1,2 [Å]* |
|---|---|---|---|---|---|
| *Co1-O2* | 2.0649 | Co2-O4 | 2.2472 | *Co4-O12* | 2.0721 |
| *Co1-O11* | 2.0762 | *Co3-O6* | 2.2328 | *Co4-O12* | 2.0833 |
| *Co1-O10* | 2.0795 | *Co3-O11* | 2.0592 | *Co5-O5* | 2.0331 |
| *Co1-O2* | 2.0997 | *Co3-O1* | 2.0330 | *Co5-O4* | 2.2381 |
| *Co1-O1* | 2.1154 | *Co4-O5* | 2.1366 | *Co5-O12* | 2.0572 |
| *Co2-O5* | 2.0474 | *Co4-O10* | 2.0956 | *Co5-O2* | 2.0735 |
| *Co2-O10* | 2.0514 | *Co4-O11* | 2.0423 | *Co5-O1* | 2.0197 |

*Table 6 Structural information for compound **3**.*

| *Formula* | *$Co_4(OH)_6(SO_4)_2[enH_2]$* |
|---|---|
| *Molar mass (g/mol)* | 592.0162 |
| *Crystal system* | Triclinic |
| *Space group* | P-1 |
| *a (Å)* | 8.3653(19) |
| *b (Å)* | 8.3880(19) |
| *c (Å)* | 10.569(3) |
| *α (°)* | 74.842(10) |
| *β (°)* | 84.498(10) |
| *γ (°)* | 83.628(9) |
| *V ($Å^3$)* | 709.65(31) |
| *Z* | 2 |

The unit cell of this crystal was drawn using the Diamond - Crystal and Molecular Structure Visualization software and can be seen along the a-axis and c-axis in figure 13 and 14, respectively.

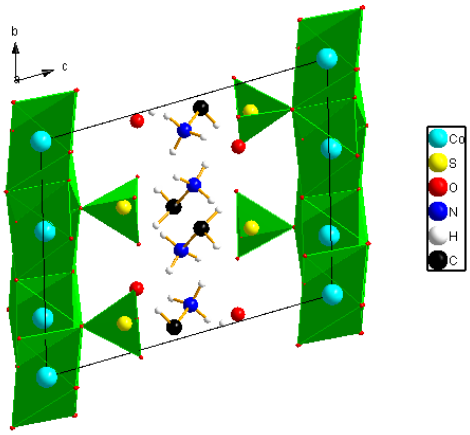


*Figure 13 Unit cell of compound **3** seen along the a-axis*

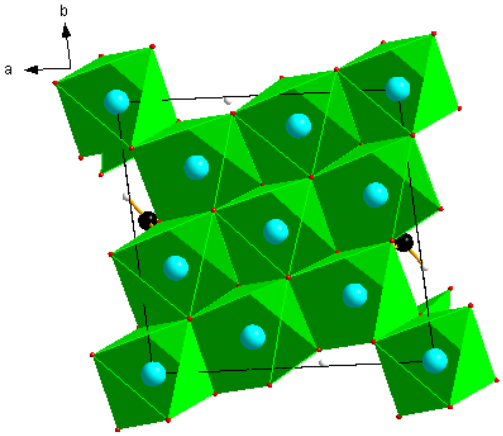


*Figure 14 Unit cell of compound **3** seen along the c-axis*

It is apparent from figure 13 that the unit cell has a layered structure. The crystal consists of layers of edge-sharing $CoO_6$ octahedra that are separated by sulphate anions and ethylenediamine molecules. The Co-O distances range from 2.02 to 2.32 Å which is consistent with $Co^{2+}$-O distances as found in for example CoO (2.13 Å). Each octahedron contains one "long" Co-O distance of, on average, 2.27 Å, one "intermediate" Co-O distance of, on average, 2.13 Å and four "short" distances of, on average, 2.06 Å, which indicates a Jahn-Teller distortion and suggests that $Co^{2+}$ ($d^7$) is in the low-spin state. The five crystallographically distinct cobalt octahedra in this crystal all show Jahn-Teller distortions.

The Jahn-Teller distortion here involves tetragonal compression of the octahedra, where the equatorial bonds are longer than the axial Co-O bonds. The cobalt cations lie on a triangular sublattice and are separated by an average distance of 3.18 Å, which indicates that there could be some strong magnetic exchange interactions.

The triangular sublattice can be seen in figure 15. The Co-O-Co bond angles are all close to 90˚ and this can also been seen in figure 15. A schematic representation of this triangular sublattice is shown in figure 16. Only the long and "intermediate" Co-O bonds are shown in this representation. These bonds form a regular pattern. The intermediate bonds in figure 16 should be "long" Co-O bonds but due to the fact that in this direction there is a short distance of only 2.7 Å between two nearby oxygen atoms, there will be electrostatic repulsion between these atoms. This causes the "long" Co-O bond to become an "intermediate" Co-O bond.

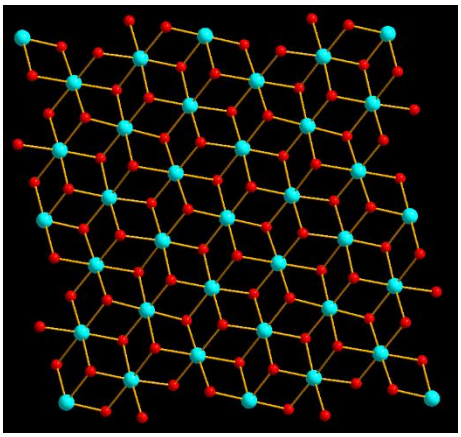

*Figure 15 Triangular sublattice. The blue spheres represent cobalt atoms and the red spheres represent oxygen atoms.*

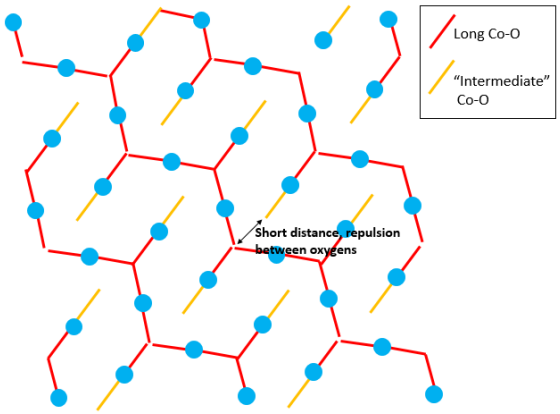


*Figure 16 Schematic representation of the triangular sublattice. The blue spheres represent cobalt atoms and the red spheres represent oxygen atoms. The short Co-O bonds are not shown in this representation.*

This structure has some similarity to the organic-inorganic hybrid crystal phenylethylammonium copper chloride, shown in figure 17, that was synthesized by Polyakov et al.[12] Layers of distorted corner-sharing $CuCl_6$ octahedral are separated by phenylethylammonium molecules. However, the copper cations form a square sublattice instead of a triangular sublattice.

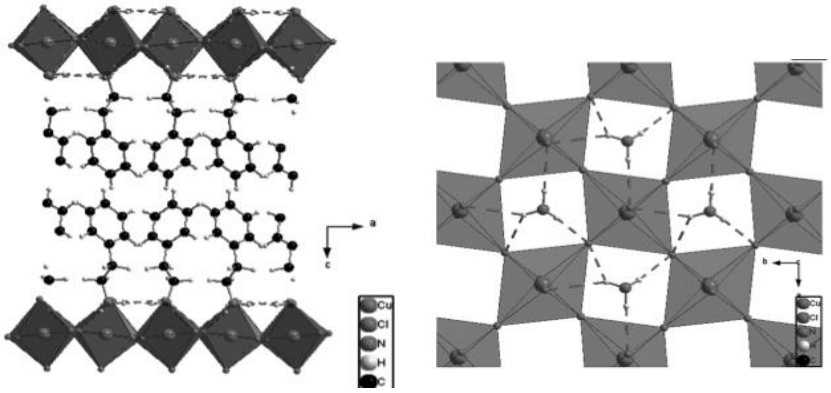

*Figure 17 The layered structure of the phenylethylammonium copper chloride crystal is shown in the upper half of the figure. The lower half of the figure shows the square sublattice formed by the copper cations.[12]*

## 4.3 Magnetic behavior

Orange crystal:

The zero-field-cooled and field-cooled magnetic susceptibility of the orange crystal was measured in an externally applied magnetic field of 1000 Oe, as shown in figure 18.
The inverse susceptibilities are plotted against temperature in figure 19.
There is no difference between the field cooled and zero-field cooled susceptibilities, which suggests that this is not a magnetically frustrated system.
The magnetic susceptibility is proportional to 1/T over the whole temperature range. A linear fit to the data intercepts the origin. This implies that θ=0 and that the material shows paramagnetic behavior without any significant exchange interactions. From this data an effective magnetic moment of $\mu_{eff}$ = 4.7 $\mu_B$ per Co atom was determined. This is close to the theoretical value of $\mu_{eff}$ = 4.9 $\mu_B$ for a system with S=2 (4 unpaired electrons) and corresponds to a high spin $Co^{3+}$ ($d^6$) complex.

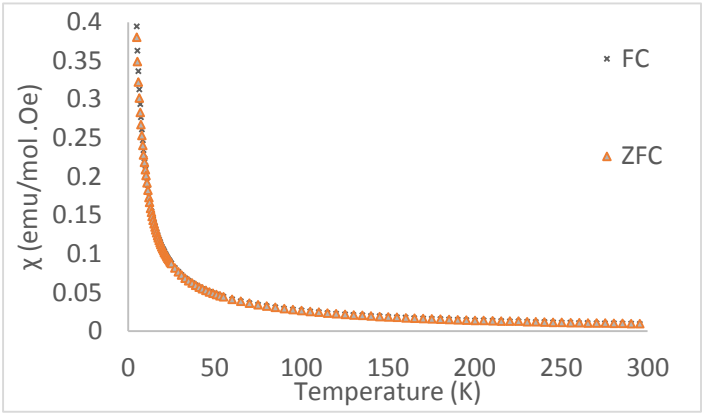


*Figure 18 The temperature dependency of the magnetic susceptibility is shown for compound **2**.*

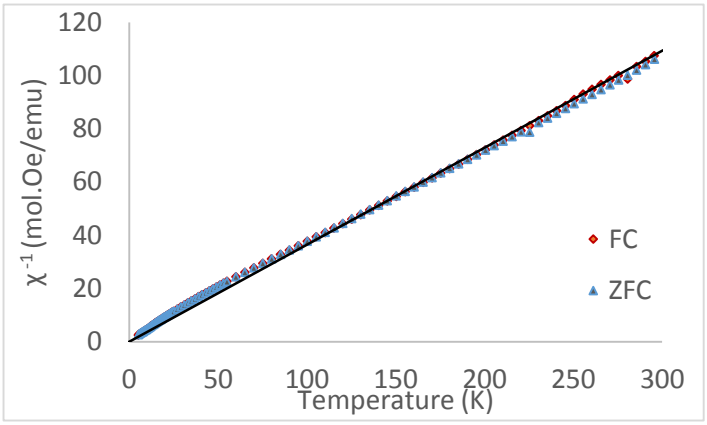


*Figure 19 The temperature dependency of the inverse magnetic susceptibility is shown for compound **2** combined with a linear fit.*

Pink crystal:

The zero-field cooled and field cooled magnetic susceptibility of a pink crystal was measured on warming in an externally applied magnetic field of 1000 Oe, as shown in figure 20. A zoomed in view of the inverse susceptibility is plotted against temperature in figure 21.
There is no difference between the field cooled and zero field cooled susceptibilities, but both show a sharp upturn below 11K suggestive of ferromagnetic order.

The magnetic susceptibility is not proportional to 1/T below 11 K. Above this temperature, the Curie-Weiss law was fitted to the paramagnetic region of the inverse magnetic susceptibility. The Weiss constant was extracted from this fit. The value of θ=11.2K confirms the presence of ferromagnetic interactions and is consistent with the onset of ferromagnetic ordering below 11K. From this data an effective magnetic moment of $\mu_{eff}$ = 2.3 $\mu_B$ per Co atom was also determined.

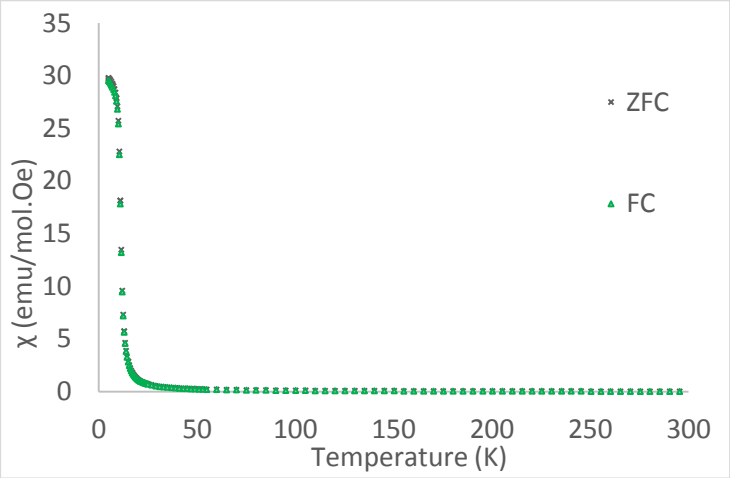


*Figure 20 The temperature dependency of the magnetic susceptibility is shown for compound **3**.*

This is somewhat larger than the theoretical value for a system with S=1/2 (1 unpaired electron), which is $\mu_{eff}$ = 1.73 $\mu_B$ per Co atom. The difference between these values is likely caused by an orbital contribution or the uncertainty in the mass of the small crystal (0.0005 g). The value of $\mu_{eff}$ corresponds to a low spin $Co^{2+}$ ($d^7$) complex, which is in agreement with the X-ray diffraction data.

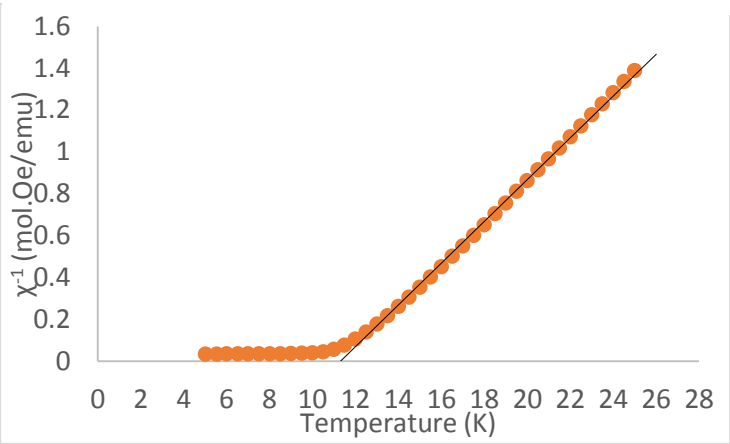


*Figure 21 The temperature dependency of the inverse magnetic susceptibility is shown for compound **3**.*

The magnetization versus applied magnetic field for the pink crystal is plotted in figure 22. The magnetization saturates at a value of 1.5 $\mu_B$ per Co atom in a field of about 2000 Oe. There is no sign of hysteresis in this crystal. This type of magnetic behavior was previously seen in a phenylethylammonium copper chloride organic-inorganic hybrid with a similar layered structure.[12] The lack of hysteresis can probably be explained by the fact that because of its layered

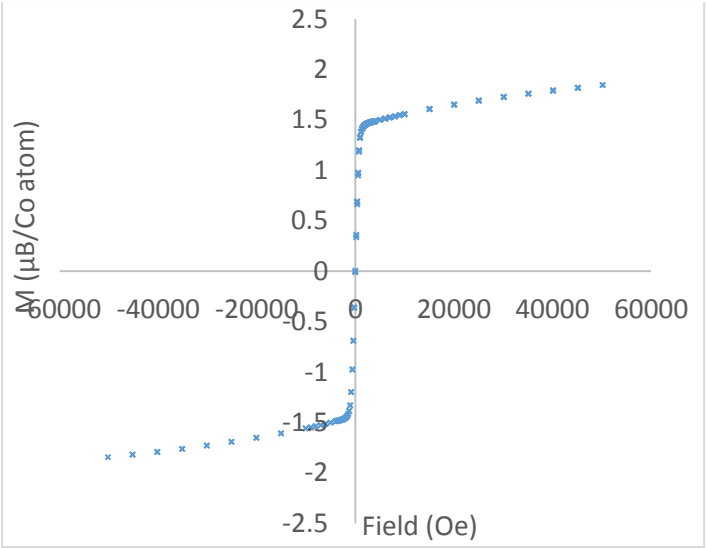


*Figure 22 The magnetization versus the field of compound **3** has been plotted.*

structure, the crystal is not a true 3D ferromagnet. The ferromagnetism is likely contained within the layers of cobalt octahedra and so this crystal is a 2D ferromagnet. The angles of the superexchange pathways (Co-O-Co) are all around 90˚which is consistent with ferromagnetic exchange.[5] Due to the octahedral distortion (Jahn-Teller distortion) every cobalt ion has a single (magnetic) electron in the $d_{z^2}$ orbital because it becomes lower in energy. The origin of the ferromagnetic ordering can also be seen in figure 16. For the oxygens where three long bonds meet, we have a situation where three half-filled $d_{z^2}$ orbitals from three different cobalt ions point at the three p-orbitals of oxygen. Since the Co-O-Co bond angles are all around 90˚ this gives rise to ferromagnetic exchange (Goodenough-Kanamori rules) and the spins on all three cobalts will be parallel. Due to the bonding pattern in the crystal structure also known as orbital ordering, the ferromagnetic order propagates throughout the layer.
The distance between adjacent layers of cobalt octahedra is over 10 Å. This distance is too large for any significant ferromagnetic exchange interactions.

## 4.4 Electrical behavior

The capacitance and dielectric loss of the crystal was measured over a range of frequencies from 100 Hz to 1 MHz and in applied magnetic fields of 0 T and 5 T. The capacitance in an applied magnetic field of 5 T had lower values over the entire temperature range but was too noisy to properly interpret and make qualitatively conclusions. Therefore, possible magnetoelectric coupling in this crystal is yet to be examined.

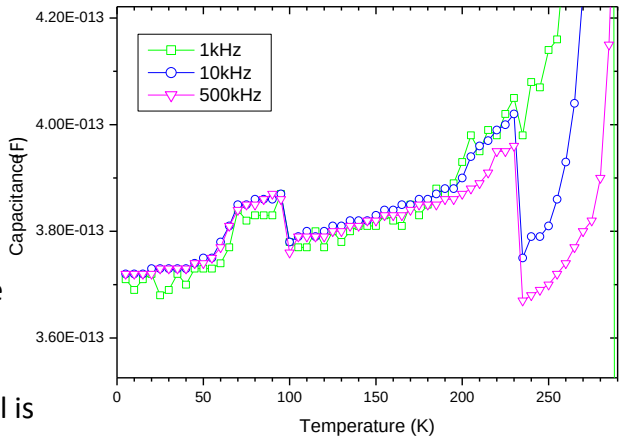


*Figure 23 The temperature dependency of the capacitance is shown for compound **3**.*

The capacitance and the loss are plotted against temperature at 1, 10 and 500 kHz in figures 23and 24. There are two temperatures in the plotted capacitance at which a sudden change is seen at every frequency. The biggest change in the capacitance (above 250 K) is probably caused by melting water absorbed on the sample surface. There is also a step-like anomaly at 90 K. In the plotted loss versus temperature graph a small peak is seen at 90 K at 10 kHz. This suggests that it is a genuine anomaly. The step in capacitance might be caused by a structural phase transition because no evidence was found for a magnetic phase transition at this temperature in the magnetic measurements.

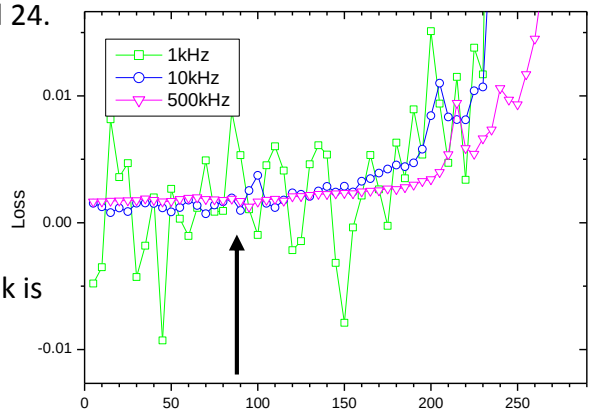


*Figure 24 The temperature dependency of the loss is shown for compound **3**.*

## 4.5 Attempted synthesis of mixed-valent iron jarosite

One type of transparent crystals (compound **4**) was obtained from attempts to synthesise the mixed-valent iron jarosite. The unit cell of the crystals was determined by single crystal x-ray diffraction and did not match any crystal found in the literature or in crystallographic databases. The dimensions of the crystals were about 0.08 mm x 0.08 mm x 0.08 mm. In figure 25 a picture of the tiny crystals is shown,

*Figure 25 Powder-like crystals of compound **4** are shown.*

which appear to the eye like a powder.
Solving the full crystal structure with single crystal x-ray diffraction proved to be difficult. However, an approximate framework was determined as shown in figure 24. Batches 1 through 3 all produced the same crystals even though the quantities of the starting materials were different in every batch. Increasing the pressure that is present during the hydrothermal synthesis did not seem to have any effect on which crystals were formed.

## 4.6 Single crystal x-ray diffraction results

An approximate crystal structure was determined using single crystal x-ray diffraction. A total of 954 reflections were collected and the structure was partially solved and refined in the spacegroup P1. R(F) was 0.1524 for 496 reflections with intensities greater than four times their standard deviations and 0.2376 for all 954 reflections. This indicates that the determined structure does not fit the data particularly well. The structural information for this crystal is shown in table 7.

*Table 7 Structural information for compound **4**.*

| *Formula* | *?* |
|---|---|
| *Crystal system* | Triclinic |
| *Space group* | P1 |
| *a (Å)* | 6.411(3) |
| *b (Å)* | 6.423(3) |
| *c (Å)* | 9.099(6) |
| *α (˚)* | 89.99(2) |
| *β (˚)* | 89.855(12) |
| *γ (˚)* | 89.733(15) |
| *V (Å$^3$)* | 374.67(35) |

The unit cell of the partial structure solution was modeled using the Diamond - Crystal and Molecular Structure Visualization software and can be seen in figure 26.

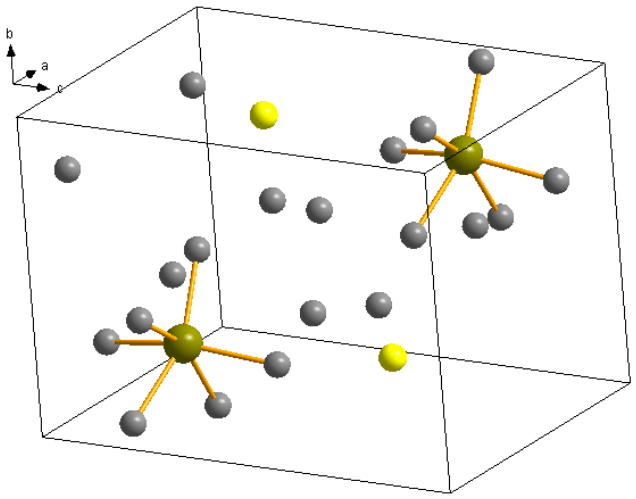


*Figure 26 The brightly yellow colored atoms represent sulfur atoms, the green atoms represent iron atoms and the gray atoms represent oxygen atoms.*

The unit cell contains two distorted $FeO_6$ octahedra. The large degree of distortion in the bond angles might be approximating rotational disorder of the octahedra. A chemically unlikely structure like this can also be a sign of a twinned crystal. However, our efforts to detect and model twinning were unsuccessful.

## 4.7 Magnetic behavior

The zero-field cooled and field cooled magnetic susceptibility of the iron crystal was measured on warming in an externally applied magnetic field of 1000 Oe, as plotted in figure 27.
The inverse field cooled susceptibility is plotted against temperature in figure 28. There was no difference between the field cooled and zero-field cooled susceptibilities, which indicates that this is not a frustrated system.

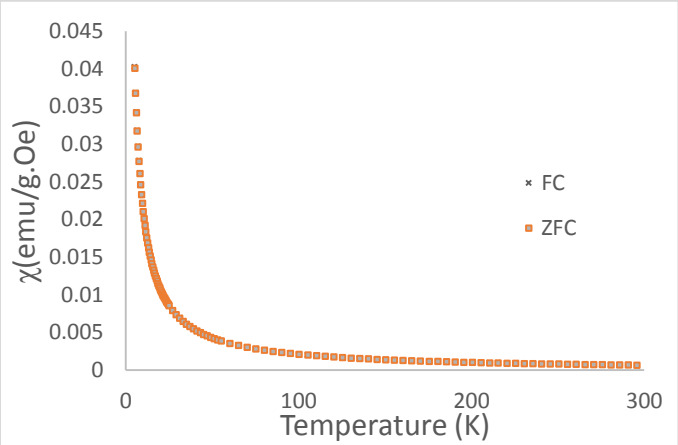


*Figure 27 The temperature dependency of the magnetic susceptibility is shown for compound **4**.*

The magnetic susceptibility seems to be proportional to 1/T over the whole temperature range. The inverse magnetic susceptibility is linear and intercepts the origin. This means that θ=0 and that the material shows paramagnetic behavior with no significant exchange interactions. We were unable to extract an effective magnetic moment due to the uncertainty in chemical composition of the crystals.

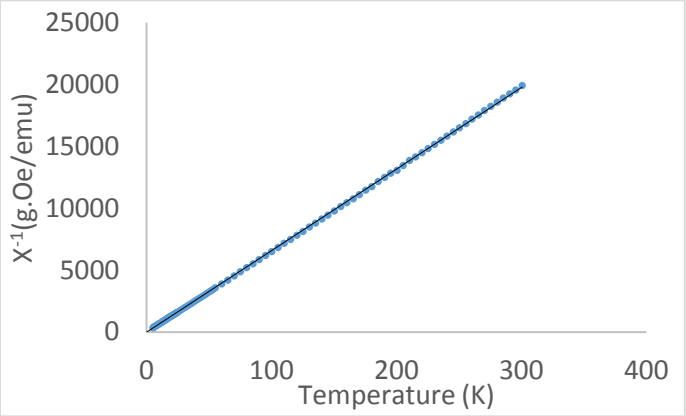


*Figure 28 The temperature dependency of the inverse magnetic susceptibility is shown for compound **4**.*

# 5. Conclusion

In this bachelor research project an attempt was made at synthesizing cobalt jarosite and mixed-valent iron jarosite crystals previously reported by Rao et al. and Powell et al. Three new crystals (two cobalt compounds and one iron compound) were synthesized that are not found in the literature or in crystallographic databases. Using different quantities of starting material, and therefore different pressures, had no impact on what crystals formed during either synthesis route. When the molar ratios of the starting materials in the synthesis of the cobalt jarosite were varied, only the orange crystal **2** was formed. The crystal structure of the two cobalt compounds **2** and **3** has been fully solved using single crystal x-ray diffraction. The pink crystal **3** has a layered structure with alternating layers of edge-sharing octahedra and organic layers of ethylenediammonium ions. The cobalt is in the +2 oxidation state (low-spin $d^7$) and lie on a triangular sublattice. The crystal structure of the orange crystals **2** consists of isolated cobalt octahedra. The cobalt is in the +3 oxidation state (high-spin $d^6$). Magnetic measurements showed that **3** orders ferromagnetically below 11 K and displays M-H curves with no hysteresis, whereas **2** shows paramagnetic behavior down to 2K, the lowest temperature measured. This behavior is consistent with the crystal structures of the compounds. The capacitance measurement of **3** shows a possible structural phase transition at 90 K. The crystal structure of the iron compound **4** has not been fully solved and only a tentative solution of the crystal structure was made. This suggested that there is rotational disorder of $FeO_6$ octahedra or unresolved twinning of the crystal. Magnetic susceptibility measurements showed that this crystal is paramagnetic down to 2K, the lowest temperature measured.

# 6. Outlook

There are several things that should still be investigated in the compounds found in this research project. The capacitance measurement that was conducted on compound **3** with an externally applied magnetic field switched on and off showed signs of magnetoelectric coupling. Capacitance measurements with an applied magnetic field should be done to see if the observed lower capacitance of the sample over the whole temperature range in a field of 5T is a genuine anomaly or not. The exact temperature that is present during synthesis is still uncertain, therefore the furnace that is used for the synthesis should be calibrated. The influence of the temperature on the crystals that are formed during synthesis should also be investigated. The magnetic susceptibility of compound **3** should be measured with the c-axis parallel to the magnetic field to see if there is a difference between the measured susceptibility of the crystal orientated parallel and perpendicular to the magnetic field. The Jahn-Teller distortion of the $CoO_6$ octahedra in this compound should be investigated more. At some temperature there should be an "orbital ordering" transition where the Jahn-Teller distortion sets in and high temperature XRD measurements should be done to find that ordering temperature. The crystal structure of compound **4** should also be solved.

# 7. Appendix

*Appendix A* *Atomic coordinates and temperature factors of compound **3***

| *Atom* | *x* | *y* | *z* | *U (Å²)* |
|---|---|---|---|---|
| *Co1* | 0.36839(9) | 0.88215(9) | -0.00757(8) | 0.0035(2) |
| *Co2* | 0.50000 | 1.50000 | 0 | 0.0033(2) |
| *Co3* | 0 | 1.00000 | 0 | 0.0036(2) |
| *Co4* | 0.12953(9) | 1.61642(9) | 0.00641(8) | 0.0036(2) |
| *Co5* | 0.25146(9) | 1.25244(9) | -0.00888(8) | 0.0034(2) |
| *S1* | 0.50245(17) | 0.62100(17) | 0.27893(14) | 0.0043(3) |
| *S2* | 0.01961(17) | 1.13089(17) | 0.27479(14) | 0.0038(3) |
| *O5* | 0.2914(5) | 1.4123(5) | 0.0975(4) | 0.0050(7) |
| *O1* | 0.2071(5) | 1.0810(5) | -0.1012(4) | 0.0045(7) |
| *O2* | 0.4054(5) | 1.0600(5) | 0.0918(4) | 0.0066(8) |
| *O4* | 0.5218(5) | 0.6702(5) | 0.1289(4) | 0.0049(7) |
| *O6* | 0.0306(5) | 1.1707(5) | 0.1247(4) | 0.0066(8) |
| *O7* | 0.3281(5) | 0.6487(5) | 0.3182(4) | 0.0092(9) |
| *O8* | 0.5609(5) | 0.4473(5) | 0.3276(4) | 0.0095(8) |
| *O9* | 0.5917(5) | 0.7330(5) | 0.3288(4) | 0.0092(9) |
| *O10* | 0.3466(5) | 1.6921(6) | -0.0960(5) | 0.0051(9) |
| *O11* | 0.1535(5) | 1.8036(5) | 0.0920(5) | 0.0047(9) |
| *O12* | -0.0934(5) | 1.5541(5) | 0.0980(4) | 0.0054(8) |
| *O13* | -0.0902(4) | 1.2628(4) | 0.3151(4) | 0.0066(8) |
| *O14* | -0.0375(5) | 0.9678(5) | 0.3304(4) | 0.0082(9) |
| *O15* | 0.1838(5) | 1.1375(5) | 0.3172(4) | 0.0076(9) |
| *N1* | 0.3284(6) | 0.8709(6) | 0.4982(5) | 0.0063(10) |
| *H1* | 0.37970 | 0.79560 | 0.45630 | 0.0090 |

*Appendix B* *Atomic coordinates and temperature factors of compound **2***

| *Atom* | *x* | *y* | *z* | *U (Å²)* |
|---|---|---|---|---|
| *Co1* | 0.50000 | 0.50000 | 0.50000 | 0.00604 |
| *S2* | 0.70082(4) | 0.72115(4) | 0.75075(4) | 0.00544 |
| *O1* | 0.66878(15) | 0.68105(14) | 0.56903(13) | 0.01170 |
| *O2* | 0.49630(14) | 0.76010(15) | 0.89157(14) | 0.00700 |
| *O5* | 0.81322(15) | 0.89913(14) | 0.68336(14) | 0.00983 |
| *O3* | 0.24172(14) | 0.57092(15) | 0.73346(14) | 0.00723 |
| *O6* | 0.82450(15) | 0.55118(14) | 0.84540(15) | 0.00868 |
| *O4* | 0.42428(17) | 0.74478(15) | 0.29038(15) | 0.01939 |
| *N1* | 0.82500(16) | 0.99283(16) | 0.25884(16) | 0.0089(2) |
| *H1* | 0.76940 | 0.89120 | 0.35740 | 0.0130 |
| *H2* | 0.72070 | 1.08400 | 0.22520 | 0.0130 |
| *H3* | 0.90600 | 1.05110 | 0.30280 | 0.0130 |
| *C1* | 0.95327(19) | 0.91523(17) | 0.08194(18) | 0.01092 |
| *H4* | 0.86600 | 0.85110 | 0.03390 | 0.0100 |
| *H5* | 1.06580 | 0.81440 | 0.11830 | 0.0100 |

## References


(1) Buurma, a. J. C.; Handayani, I. P.; Mufti, N.; Blake, G. R.; Van Loosdrecht, P. H. M.; Palstra, T. T. M. *J. Solid State Chem.* **2012**, *195*, 50–54.

(2) Cheong, S.-W.; Mostovoy, M. *Nat. Mater.* **2007**, *6*, 13–20.

(3) Curie, P. *J. Phys.* **1894**, *3*, 393–415.

(4) Dai, D.; Whangbo, M. H. *J. Chem. Phys.* **2004**, *121*, 672–680.

(5) Delaney, K. T.; Mostovoy, M.; Spaldin, N. a. *Phys. Rev. Lett.* **2009**, *102*, 1–4.

(6) Haas, O.; Struis, R. P. W. J.; McBreen, J. M. *J. Solid State Chem.* **2004**, *177*, 1000–1010.

(7) Hauptman, Z.; Kaczer, J.; Shalnikova, T. *Czechoslov. J. Phys. B* **1968**, *18*, 734–737.

(8) Hoppe, J. I. *J. Chem. Educ.* **1972**, *49*, 505.

(9) Kimura, T.; Goto, T.; Shintani, H.; Ishizaka, K.; Arima, T.; Tokura, Y. *Nature* **2003**, *426*, 55–58.

(10) Mangalam, R. V. K.; Ray, N.; Waghmare, U. V.; Sundaresan, A.; Rao, C. N. R. *Solid State Commun.* **2009**, *149*, 1–5.

(11) Nan, C. W.; Bichurin, M. I.; Dong, S.; Viehland, D.; Srinivasan, G. *J. Appl. Phys.* **2008**, *103*, 1–36.

(12) Polyakov, A. O.; Arkenbout, A. H.; Baas, J.; Blake, G. R.; Meetsma, A.; Caretta, A.; Van Loosdrecht, P. H. M.; Palstra, T. T. M. *Chem. Mater.* **2012**, *24*, 133–139.

(13) Powell, A. V.; Leyva-Bailen, P.; Vaqueiro, P.; Sanchez, R. D. *Chem. Mater.* **2009**, *21*, 4102–4104.

(14) Rao, C.; Paul, G.; Choudhury, A.; Sampathkumaran, E.; Raychaudhuri, A.; Ramasesha, S.; Rudra, I. *Phys. Rev. B* **2003**, *67*, 1–5.

(15) Schmid, H. *Ferroelectrics* **1994**, *162*, 317–338.

(16) Spaldin, N. A.; Fiebig, M. *Science* **2005**, *309*, 391–392.